Research Square

Preprints are preliminary reports that have not undergone peer review.
They should not be considered conclusive, used to inform clinical practice,
or referenced by the media as validated information.

Calibration limited quantum advantage in dose constrained biomolecular absorption spectroscopy

Baldo Alberto Luigi Dalporto

baldo.dalporto@intec.edu.do

Instituto Tecnológico de Santo Domingo

Sabine Mary

Instituto Tecnológico de Santo Domingo

Santiago Gallur

Instituto Tecnológico de Santo Domingo

Research Article

Keywords: quantum metrology, biomolecular spectroscopy, absorption estimation, nuisance parameters, photon dose, spectral calibration, Fisher information

Posted Date: October 30th, 2026

DOI: https://doi.org/10.21203/rs.3.rs-11376366/v1

License: This work is licensed under a Creative Commons Attribution 4.0 International License.
Read Full License

Additional Declarations: No competing interests reported.

Calibration limited quantum advantage in dose constrained biomolecular absorption spectroscopy

Baldo Alberto Luigi Dalporto[1], Sabine Mary[2] and Santiago Gallur[2]

Instituto Tecnológico de Santo Domingo (INTEC), Santo Domingo, Dominican Republic

[1] Department of Engineering, Instituto Tecnológico de Santo Domingo (INTEC), Santo Domingo, Dominican Republic

[2] Area of Social Sciences and Humanities, Instituto Tecnológico de Santo Domingo (INTEC), Santo Domingo, Dominican Republic

* **Correspondence: Baldo Alberto Luigi Dalporto**, baldo.dalporto@intec.edu.do

ORCID: Baldo Alberto Luigi Dalporto, 0009-0008-8719-1562; Sabine Mary, 0009-0004-3488-9511; Santiago Gallur, 0000-0001-6287-7340

Abstract

Quantum optical probes can improve absorption measurements per specimen photon, but uncertain throughput can obscure the concentration advantage. We analyze two-wavelength concentration estimation with unknown common throughput, a local absorbed-photon budget and independently calibrated relative spectral response. For number-state and coherent probes, exact zero-background photon-counting Fisher bounds yield closed-form optimal exposure allocations. Finite spectral-calibration information introduces an additive concentration-variance floor. Consequently, the optimized fixed-dose variance advantage approaches unity as specimen exposure increases while calibration information remains fixed. We derive an explicit calibration requirement for a prescribed advantage and a joint allocation rule when sample exposure and calibration share an accounting budget. Unlabelled Poisson background is treated through an explicit likelihood and a separately identified first-order estimator approximation. Reproducible dimensionless calculations verify the analytical allocations and illustrate the calibration-limited regime. The contribution is a calibration-aware design criterion for linear biomolecular absorption assays, not a universal quantum limit or a clinical performance claim. The model applies to a known dominant absorber with a known path

length and negligible scattering. It distinguishes improvements attainable through photon statistics from uncertainty that instead requires better spectral calibration.

Keywords: quantum metrology; biomolecular spectroscopy; absorption estimation; nuisance parameters; photon dose; spectral calibration; Fisher information

1 Introduction

Optical concentration measurements underpin biomolecular quantification, biochemical reaction monitoring and characterization of photosensitive preparations. The optical signal is generated by a physical interaction between a probe and a specimen, so increasing the illumination is not always an acceptable route to smaller statistical uncertainty. Quantum optical metrology addresses this constraint by modifying the photon statistics or correlations of the probe. Experimental studies have demonstrated quantum-enhanced measurements in biological systems, including particle tracking and microscopy [1, 2]. These achievements motivate a precise question: which technical uncertainty must be controlled before an improvement in photon statistics translates into a smaller uncertainty in a molecular quantity?

The distinction matters because transmission is rarely the final measurand. A detector records photons after sample absorption, collection loss and detector inefficiency have all acted. A change in measured throughput may therefore reflect a change in concentration, a change in coupling, or a change in spectral responsivity. At one wavelength, unknown multiplicative throughput and unknown concentration are not separately identifiable in the model considered here. Two wavelengths can remove a common multiplicative factor, but only if their relative response is known or independently constrained. No amount of photon-number squeezing resolves a structural ambiguity between an analyte spectrum and an unrestricted instrumental spectrum.

The quantum advantage of number states for loss estimation is established [3, 4]. Per-sample-photon comparisons, twin-beam estimators and biological absorption experiments already provide

operational benchmarks [5, 6, 7]. Allen and colleagues showed that optimizing the interaction length materially changes the coherent-state benchmark in absorbance estimation [8]. Woodworth and colleagues treated transmission estimation under loss and imperfect detection and later demonstrated an appropriate quantum Cramér–Rao benchmark experimentally [9, 10]. Goldberg and Heshami investigated transmission measurements with dark counts and nuisance parameters [11]. Recent studies have further developed weak-absorption estimation with correlated photons [12] and adaptive multiparameter sensing that addresses probe and calibration uncertainty [13]. Accordingly, neither the suppression of number fluctuations, the existence of loss, nor the importance of calibration is presented here as a new discovery.

Our question is narrower. For a differential two-wavelength concentration measurement, how should the specimen exposure be allocated when common throughput is unknown, and how much independent spectral calibration is needed to retain a specified quantum advantage? We address this question through an explicitly defined statistical model. The main result combines nuisance elimination, specimen-dose optimization and finite calibration information in one concentration-variance expression. It yields a testable design inequality: a requested variance advantage is feasible only if the relative-response calibration is sufficiently informative for the selected specimen dose. We additionally separate a sample-dose budget from an instrument-accounting budget, preventing calibration photons that never reach the specimen from being misclassified as biological exposure.

The work is theoretical. Its evidence consists of likelihood calculations, analytical derivations, limiting-case analysis and reproducible numerical checks. No biological specimens, patient measurements or prototype experiments are reported. The intended biomedical and biotechnological setting is transmission spectroscopy of a known analyte in a preparation for which a linear Beer–Lambert description is defensible. Application to intact tissue, mixtures with unknown spectra or clinical decision making would require a different forward model and independent validation.

2 Physical and statistical methods

2.1 Linear absorption and the measured optical channel

Let c denote analyte concentration and let $k_i > 0$ be the known absorption coefficient per unit concentration at wavelength $i \in \{1,2\}$, including the known optical path length. The sample transmission and the probability that an incident photon is detected are

$$t_i(c) = \exp(-k_i c), \qquad p_i = \eta q_i t_i(c), \qquad 0 < p_i < 1. \qquad (1)$$

Here η is an unknown common throughput factor and q_i is a known relative spectral factor. The admissible parameter domain requires $\eta q_i \leq 1$. The baseline model places these technical losses after the specimen. Equivalently, N_i below must be the number of photons actually incident on the specimen, not photons emitted upstream of an uncharacterized lossy preparation stage. An imperfect source that does not deliver the assumed number statistics to the specimen must be modeled separately.

When tabulated molar extinction coefficients use decimal absorbance, the conversion is $k_i = \ln(10)\epsilon_i \ell$, with compatible units for ϵ_i, path length ℓ and concentration c. Thus, $k_i c$ is dimensionless. This conversion prevents a common factor-of-$\ln(10)$ error. Equation (1) assumes linear, nonsaturating absorption; known path length; stationary concentration within an acquisition; and negligible scattering and reflection within the modeled sample channel. It is not a general radiative-transfer model.

The quantum-optical description of each loss channel is

$$\hat{a}_{i,\mathrm{out}} = \sqrt{p_i}\,\hat{a}_{i,\mathrm{in}} + \sqrt{1 - p_i}\,\hat{v}_i, \qquad (2)$$

where $\hat{v}_i$ is an independent vacuum environment mode. Equation (2) preserves the bosonic commutator. A number state incident on this channel gives binomial counting statistics; a coherent state gives Poisson statistics with a reduced mean. These facts establish the connection between the

quantum probe and the statistical model. No entanglement is needed for the comparison developed here.

2.2 Resource accounting and the coherent benchmark

For the number-state strategy, N_i denotes an integer number of incident photons whose total is known. It can represent an ideal Fock pulse or a sequence of ideal single-photon trials with all specimen exposures included. For the coherent strategy, N_i is the known mean incident photon number. The comparison uses the same wavelengths, path length, technical throughput, relative-response information and specimen-dose definition. It does not compare a calibrated quantum apparatus with an uncalibrated classical apparatus.

Define the local exposure cost per incident photon by

$$d_i = w_i[1 - t_i(c_0)], \qquad D = \sum_{i=1}^{2} N_i\, d_i, \qquad w_i > 0. \qquad (3)$$

The design point c_0 is specified before the acquisition. For $w_i = 1$, D is the expected number of sample-absorbed photons at that point. For $w_i = hc/\lambda_i$, it is absorbed optical energy. A wavelength-dependent damage weight would require biological evidence and is not supplied by this theory. Phototoxicity depends on more than absorbed energy, including exposure timing, photochemistry and the biological endpoint [14]. We therefore call D an exposure or absorbed-dose resource, not a validated safety threshold.

The resource is an expectation, not a hard cap on realized photon absorption. Both strategies exhibit random absorption, and the coherent strategy also fluctuates in its incident photon number. An application requiring a probabilistic upper bound on injury would need to constrain exposure tails and the biological response. Source pump energy, reference-arm photons, acquisition time and detector complexity are outside D unless explicitly introduced into a separate instrument budget.

2.3 Counting likelihoods and regularity

With background absent, the independent count likelihoods are

$$Y_i^{\mathrm{num}} \sim \mathrm{Binomial}(N_i, p_i), \qquad Y_i^{\mathrm{coh}} \sim \mathrm{Poisson}(N_i p_i). \qquad (4)$$

Let $u = \ln\eta$ and $\boldsymbol{\theta} = (c, u)$. The Fisher information of an observed likelihood is

$$F_{ab} = \mathbb{E}_{\boldsymbol{\theta}}[\partial_a \ln L \; \partial_b \ln L]. \qquad (5)$$

For regular locally unbiased estimation, the covariance is bounded by the inverse information matrix. The bound is local: it is evaluated at a parameter point, and the experiment's N_i are held fixed when derivatives are taken. Differentiating an optimized design $N_i(c)$ as if it were an observed dependence on unknown concentration would add spurious information. A pilot acquisition can select a design point, but its specimen exposure and uncertainty must then be counted.

The present calculations concern Fisher information for the stated measurements. We do not prove a universal optimum over all quantum probes, adaptive strategies or collective measurements. The number-state output is diagonal in a parameter-independent number basis, so photon counting extracts its available channel information. For the coherent benchmark, photon counting is a natural attainable loss measurement. These observations do not eliminate the need to state the resource constraint and nuisance model when invoking a quantum bound [15].

3 Analytical results

3.1 Eliminating common throughput

For either strategy, define the information weight

$$g_i^{\mathrm{num}} = \frac{N_i p_i}{1 - p_i}, \qquad g_i^{\mathrm{coh}} = N_i p_i. \qquad (6)$$

Because $\partial_c \ln p_i = -k_i$ and $\partial_u \ln p_i = 1$, the information matrix is

$$F = \sum_{i=1}^{2} g_i \begin{pmatrix} k_i^2 & -k_i \\ -k_i & 1 \end{pmatrix}. \qquad (7)$$

Its determinant is $g_1 g_2 (k_1 - k_2)^2$. Therefore, concentration and common throughput are locally identifiable precisely when both channels carry positive information and $\Delta k = k_1 - k_2 \neq 0$.

Inverting Eq. (7), or eliminating u by a Schur complement, gives

$$V_c \equiv [F^{-1}]_{cc} = \frac{g_1^{-1} + g_2^{-1}}{(\Delta k)^2}. \qquad (8)$$

The quantity V_c is the concentration variance lower bound, not the measured variance of a finite dataset. The result makes the throughput penalty explicit. If throughput were known, the scalar information would be $\sum_i g_i k_i^2$. Unknown throughput instead leaves only the differential spectral information. A wavelength pair with nearly identical absorptivities is ill-conditioned even if each wavelength separately has a large absorption slope.

For counts sufficiently far from zero and the boundary, an asymptotically efficient estimator follows from the log ratio,

$$\hat{c} = -\frac{1}{\Delta k} \ln \left[\frac{Y_1/(N_1 q_1)}{Y_2/(N_2 q_2)} \right]. \qquad (9)$$

The common throughput cancels. The delta-method variance of Eq. (9) equals Eq. (8) at leading order. The logarithm introduces finite-count bias, and zero counts make the displayed estimator undefined. A full constrained likelihood fit or an explicitly regularized estimator is needed in such regimes; discarding zero-count trials silently is not an acceptable analysis.

3.2 Optimal allocation of absorbed exposure

$$A_i^{\mathrm{num}} = \frac{1 - p_i}{p_i}, \qquad A_i^{\mathrm{coh}} = \frac{1}{p_i}, \qquad S_s = \sum_{i=1}^{2} \sqrt{A_i^s d_i}\,, \qquad (10)$$

where s denotes the chosen strategy. At a fixed design point with $d_i > 0$, minimizing $\sum_i A_i^s / N_i$ under Eq. (3) gives

$$N_i^{s,*} = \frac{D\sqrt{A_i^s / d_i}}{S_s}, \qquad f_i^{s,*} \equiv \frac{N_i^{s,*} d_i}{D} = \frac{\sqrt{A_i^s d_i}}{S_s}. \qquad (11)$$

The proof follows either from a Lagrange multiplier or from Cauchy–Schwarz:

$$\left(\sum_i \frac{A_i^s}{N_i}\right)\left(\sum_i N_i\, d_i\right) \geq \left(\sum_i \sqrt{A_i^s d_i}\right)^2. \qquad (12)$$

The optimized variance bound is consequently

$$V_{c,s}^* = \frac{S_s^2}{D(\Delta k)^2}. \qquad (13)$$

Continuous N_i are used for design. Number-state implementations require integer allocations, for which direct local search or rounding followed by a budget check supplies a feasible design. Rounding cannot be used to claim an exact finite-integer optimum.

A fair optimized variance advantage is

$$G_0 = \frac{V_{c,\mathrm{coh}}^*}{V_{c,\mathrm{num}}^*} = \frac{S_{\mathrm{coh}}^2}{S_{\mathrm{num}}^2}. \qquad (14)$$

Both strategies optimize their own allocation. Since $A_i^{\mathrm{num}} < A_i^{\mathrm{coh}}$ for interior probabilities, $G_0 > 1$ in this ideal model. It is a variance ratio; the corresponding standard-deviation ratio is $\sqrt{G_0}$. At the same fixed allocation, the variance-bound difference has the particularly simple form

$$V_{c,\mathrm{coh}} - V_{c,\mathrm{num}} = \frac{N_1^{-1} + N_2^{-1}}{(\Delta k)^2}. \qquad (15)$$

Equation (15) does not imply that the relative advantage is independent of loss: each individual variance increases as throughput decreases. In the low-throughput limit $p_i \to 0$, the relative advantage tends to unity. Equations (11)–(14) also exclude a free-dose loophole: if an exactly

nonabsorbing reference wavelength has $d_i = 0$, the pure specimen-dose constraint fails to limit its photons. A finite instrument photon or time budget must then be added, rather than applying Eq. (11) at a singular point.

3.3 Relative spectral calibration and identifiability

A common multiplicative drift is an idealization. To allow residual relative-response error, use

$$\ln p_1 = u + \ln q_1 - k_1 c + r/2, \qquad \ln p_2 = u + \ln q_2 - k_2 c - r/2. \qquad (16)$$

The parameter r is an unknown residual log ratio. It is local and small enough that both probabilities remain physical. The detected spectral contrast now contains $r - \Delta k\, c$. With only two photon-count channels and unrestricted r, concentration is unidentifiable: a local change in c within the admissible parameter domain can be compensated by a change in relative throughput and common scale. More photons sharpen the same ambiguous contrast without resolving its interpretation.

Suppose an independent calibration yields

$$Z \sim \mathcal{N}(r, \sigma_r^2), \qquad J_r = \sigma_r^{-2}, \qquad (17)$$

with known variance. This is an auxiliary likelihood, not a Bayesian prior. It can represent a repeated reference measurement whose error model has been established independently. After eliminating u, the information for (c, r) is

$$F_{c,r} = h \begin{pmatrix} (\Delta k)^2 & -\Delta k \\ -\Delta k & 1 \end{pmatrix} + \begin{pmatrix} 0 & 0 \\ 0 & J_r \end{pmatrix}, \qquad h = \frac{g_1 g_2}{g_1 + g_2}. \qquad (18)$$

A second inversion produces the central calibration-aware bound,

$$V_{c,s}^*(D, J_r) = \frac{S_s^2/D + 1/J_r}{(\Delta k)^2}. \qquad (19)$$

The additive term is exact at Fisher-information level for the specified auxiliary likelihood. More generally, the same expression holds for an independent scalar calibration likelihood with Fisher information J_r, subject to the regularity assumptions. An arbitrary reported calibration error bar cannot automatically be substituted for $1/J_r$. A variance estimate, a systematic bound and inverse Fisher information describe different objects.

At leading order, the corresponding calibrated log-ratio estimator is

$$\hat{c} = \frac{Z - \ln[Y_1/(N_1 q_1)] + \ln[Y_2/(N_2 q_2)]}{\Delta k}. \qquad (20)$$

If the calibration has a residual bias $b_r = \mathbb{E}[Z] - r$, the induced concentration bias is $b_r/\Delta k$, and its squared value contributes to mean-squared error. If calibration is ignored altogether, Eq. (9) has the opposite-sign bias $-r/\Delta k$. A quantum noise reduction does not suppress either bias.

3.4 A calibration requirement for retained quantum advantage

Let $C = S_{\mathrm{coh}}^2$ and $Q = S_{\mathrm{num}}^2$, evaluated with the same physical parameters. The optimized variance ratio becomes

$$G(D, J_r) = \frac{C + D/J_r}{Q + D/J_r}. \qquad (21)$$

At fixed calibration information, G decreases monotonically from its ideal value C/Q toward unity as exposure increases. The two strategies approach the same calibration floor. This result does not mean quantum light becomes statistically worse; it means the remaining quantum benefit becomes a diminishing fraction of total uncertainty.

For a desired variance advantage $G_{\mathrm{tar}} > 1$, Eq. (21) gives

$$\frac{1}{J_r} \leq \frac{C - G_{\mathrm{tar}} Q}{D(G_{\mathrm{tar}} - 1)}, \qquad C > G_{\mathrm{tar}} Q. \qquad (22)$$

The second inequality expresses feasibility: no finite calibration can achieve a target larger than the zero-calibration-error gain. Equality at the ideal target requires infinite calibration information. For the Gaussian model, Eq. (22) is a requirement on σ_r^2. It can be evaluated before selecting an expensive quantum source. When the available calibration fails this requirement, improving the relative spectral response can be more consequential than further reducing probe number noise.

A second design criterion follows from a target concentration variance V_{tar}. The efficient-asymptotic inverse-Fisher benchmark admits a finite dose only if $V_{\mathrm{tar}}(\Delta k)^2 > 1/J_r$, in which case

$$D_s \geq \frac{S_s^2}{V_{\mathrm{tar}}(\Delta k)^2 - 1/J_r}. \qquad (23)$$

This is an inverse-Fisher dose benchmark, not a finite-sample performance guarantee. The same calibration must be used in both strategies when interpreting this as an exposure reduction. Equation (23) exposes an absolute floor that cannot be overcome by increasing the sample illumination.

3.5 Joint specimen and calibration resource allocation

Calibration may be improved using resources that do not illuminate the specimen. Let M be the number of equivalent independent calibration acquisitions, each providing information $j_r > 0$, and let $B = D + \kappa M$ be a common accounting budget. The coefficient $\kappa > 0$ converts calibration acquisitions into the selected accounting units. It is not a biological absorption coefficient. For a chosen strategy, the dimensionless numerator of the variance is $S_s^2/D + 1/(j_r M)$.

Optimizing over positive D and M gives

$$D_s^* = \frac{BS_s}{S_s + \sqrt{\kappa/j_r}}, \qquad \kappa M_s^* = \frac{B\sqrt{\kappa/j_r}}{S_s + \sqrt{\kappa/j_r}}, \qquad (24)$$

and

$$V_{c,s}^{*,B} = \frac{\left[S_s + \sqrt{\kappa/j_r}\right]^2}{B(\Delta k)^2}. \qquad (25)$$

A better photon-counting coefficient changes the optimal allocation between sample measurement and calibration. In particular, when calibration is expensive or weakly informative, both strategies devote a larger fraction of the accounting budget to it and their relative advantage is compressed. These results are local continuous allocations. They do not assume a particular calibration apparatus or assert that its information scales indefinitely without drift or saturation.

3.6 Finite background and a transparent attainable approximation

For unlabelled background, let $B_i \sim \mathrm{Poisson}(b_i)$ be independent of the signal, and let $K_i \sim \mathrm{Poisson}(m_i b_i)$ be an independent dark acquisition with exposure ratio $m_i > 0$. The measured signal-window count is $Y_i = X_i + B_i$, and b_i is unknown. The background-corrected count is $T_i = Y_i - K_i/m_i$.

Its first two moments are exact:

$$\mathbb{E}[T_i] = N_i p_i, \qquad \mathrm{Var}(T_i) = N_i p_i v_i + b_i(1 + m_i^{-1}), \qquad (26)$$

where $v_i = 1 - p_i$ for a number-state signal and $v_i = 1$ for a coherent signal. When $\mathrm{Var}(T_i)/(N_i p_i)^2 \ll 1$, the parameters are interior and T_i is positive with high probability, substituting T_i for Y_i in Eq. (20) gives the leading variance

$$\mathrm{Var}(\hat{c}) \simeq \frac{1}{(\Delta k)^2}\left[\sum_i \left(\frac{A_i^s}{N_i} + \frac{b_i(1 + m_i^{-1})}{N_i^2 p_i^2}\right) + \sigma_r^2\right]. \qquad (27)$$

Equation (27) is the first-order delta-method variance approximation for a specified estimator under its regular regime. For fixed b_i, its displayed background term is of order N_i^{-2}, as are omitted nonlinear logarithm corrections; the expression is therefore not a complete second-order expansion. It is not asserted to be the exact Cramér–Rao bound for a binomial signal convolved with Poisson noise. For that model, the signal-window likelihood is

$$P(Y_i = y) = \sum_{x=0}^{\min(N_i, y)} \binom{N_i}{x} p_i^x (1 - p_i)^{N_i - x} \frac{e^{-b_i} b_i^{y-x}}{(y-x)!}. \qquad (28)$$

The exact Fisher matrix must be computed from this likelihood jointly with the dark and spectral-calibration likelihoods. Treating the inverse of the count variance as exact Fisher information would be incorrect in general. In the coherent case, Y_i is Poisson with mean $N_i p_i + b_i$, and the background-nuisance calculation is simpler. The distinction between the two likelihoods must be retained even when their high-count moment approximations are close.

For fixed acquisition-window background b_i, the exposure objective in Eq. (27) contains $A_i/N_i + H_i/N_i^2$, where $H_i = b_i(1 + m_i^{-1})/p_i^2$. It is convex for $N_i > 0$. The stationarity condition is

$$\lambda d_i = \frac{A_i}{N_i^2} + \frac{2H_i}{N_i^3}. \qquad (29)$$

Thus a one-dimensional multiplier search can allocate dose, but the square-root formula in Eq. (11) is no longer exact for this approximate objective. If additional photons are obtained by extending acquisition time, b_i generally changes with N_i; the background-versus-time relation must then be incorporated before optimization. The present paper does not claim experimental validation of Eq. (27).

4 Reproducible numerical illustrations

4.1 Dimensionless design and verification protocol

To illustrate the analytical results without inventing biomarker spectra, we introduce a dimensionless concentration $x = c/c_{\mathrm{ref}}$ and select dimensionless coefficients $k_i c_{\mathrm{ref}} = (1, 0.25)$. In the figures these scaled coefficients are denoted simply by k_i. We set $q_1 = q_2 = 1$, $w_1 = w_2 = 1$ and evaluate the baseline at $r = 0$. These choices are synthetic model parameters, not measured absorption coefficients of a named protein, metabolite or tissue. A real concentration uncertainty is

recovered by multiplying the dimensionless standard deviation by c_{ref} after establishing the relevant spectrum and path length.

The reproducibility package contains a standalone Python script, numerical CSV files and vector and raster versions of all figures. The computations use Python 3.12.14, NumPy 2.3.5, SciPy 1.17.0 and Matplotlib 3.10.8. There is no stochastic simulation and therefore no random seed, excluded experimental observation or Monte Carlo acceptance rate. The illustrated curves are local bounds, not sampled estimator performance.

We checked the exposure-allocation result on 960 cases: 24 logarithmically spaced concentrations from 0.01 to 8, 20 efficiencies from 0.05 to 0.98 and both probe strategies, at $D = 1000$. For each case, an independent bounded scalar minimizer varied the fraction of absorbed dose assigned to the first wavelength. We also inverted the 2×2 Fisher matrix directly and checked the dose constraint. The largest relative differences from the analytical optimum were 1.56×10^{-15} for the minimized objective and 1.45×10^{-15} for Fisher inversion. The minimizing allocation itself agreed within 6.81×10^{-9} in absolute dose fraction. Eight additional direct 3×3 Fisher inversions checked the calibration formula over $D = 10$ to 10^7, with maximum relative discrepancy 4.35×10^{-13}. An additional 1,800 numerical joint-budget optimizations checked Eqs. (24)–(25), with maximum relative objective discrepancy 1.03×10^{-13}; 81 target-gain checks agreed within 2.23×10^{-16}. These numerical agreements verify the implementation and algebra for the tested model; they do not establish biological validity.

4.2 Loss and optimized exposure allocation

Figure 1 shows the separately optimized coherent-to-number-state variance ratio. High transmission and efficient detection favor the number-state strategy, whereas low detection probabilities suppress its relative benefit. This follows directly from the convergence of $(1 - p_i)/p_i$ and $1/p_i$ when p_i is small. The apparent large gain near low absorption and high efficiency is conditional on exact incident number statistics and local interior inference. The zero-absorption boundary, at which the selected absorbed-dose resource degenerates, is not plotted.

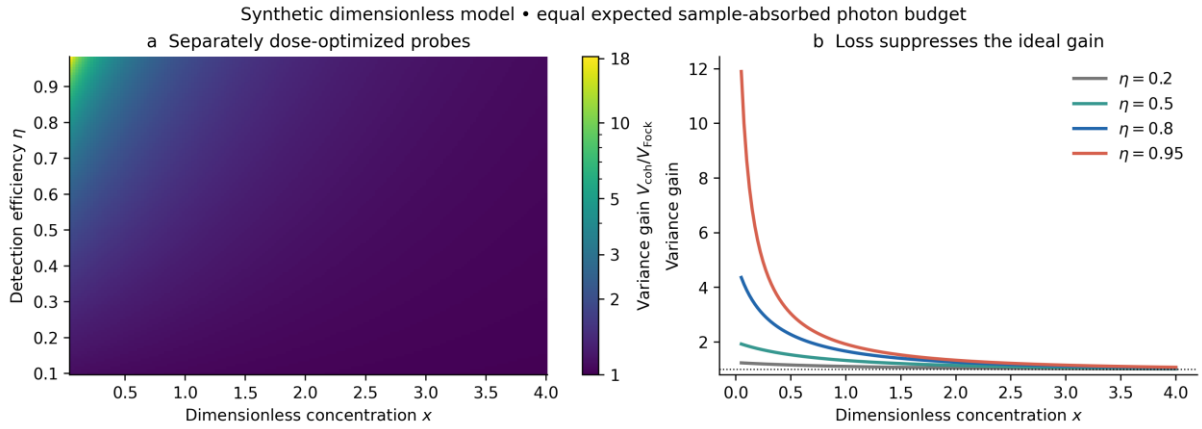


Figure 1. Loss dependent quantum variance advantage. Optimized coherent-to-number-state concentration variance bounds at equal expected absorbed-photon budget. The left panel uses a logarithmic color scale; the right panel gives selected throughput cuts. Parameters are synthetic and dimensionless. Each strategy uses its own optimal allocation. The zero-dose boundary is excluded.

The absorbed-dose fraction and the incident-photon fraction are different design quantities (Fig. 2). At $x = 0.7$ and $\eta = 0.8$, the coherent strategy allocates 69.72% of absorbed dose to the more strongly absorbing wavelength; the number-state strategy allocates 75.72%. The corresponding products DV_x are 4.634726 and 2.368102. The ideal optimized variance gain is 1.957148, corresponding to a standard-deviation gain of 1.398981. These are dimensionless theoretical ratios, not a reported biomarker detection limit.

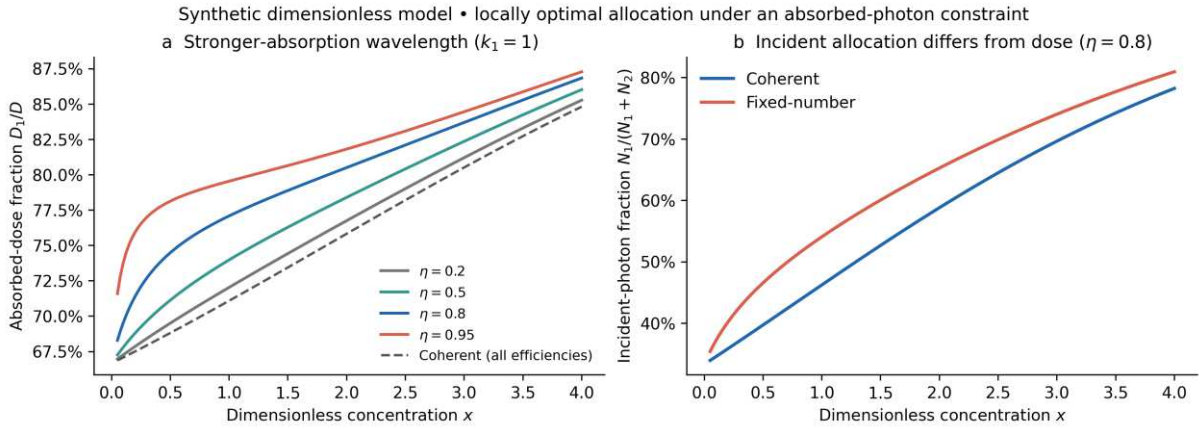


Figure 2. Optimal specimen exposure allocation. The left panel gives the fraction of absorbed photons assigned to wavelength 1 for several efficiencies. The coherent fraction is independent of the common efficiency in this model. The right panel gives incident-photon fractions at $\eta = 0.8$. The distinction matters because absorption differs between wavelengths.

4.3 Calibration limited performance

For an independent relative log-response calibration with $\sigma_r = 0.01$, the variance floor at the same illustrative point is 1.77778×10^{-4} and its standard-deviation scale is 0.0133333 in x. The statistical contribution equals this floor at approximately $D = 26{,}070$ for coherent probes and $D = 13{,}321$ for number-state probes. The number-state strategy reaches the calibration-limited regime at a smaller specimen exposure, consistent with its smaller statistical coefficient.

Figure 3 plots both the total local uncertainty and the retained variance advantage. Increasing D improves the statistical term but does not improve an independently fixed calibration. For example, at $D = 10{,}000$, retaining a variance gain of 1.5 requires $\sigma_r \leq 0.011036$; $\sigma_r = 0.01$ gives a total gain of 1.54672. This makes the calibration requirement in Eq. (22) a quantitative instrument-design condition rather than a qualitative warning. The figures do not include background, state-preparation defects or a biological damage model; Eq. (27) identifies how finite background can be introduced without misrepresenting the exact noiseless bound.

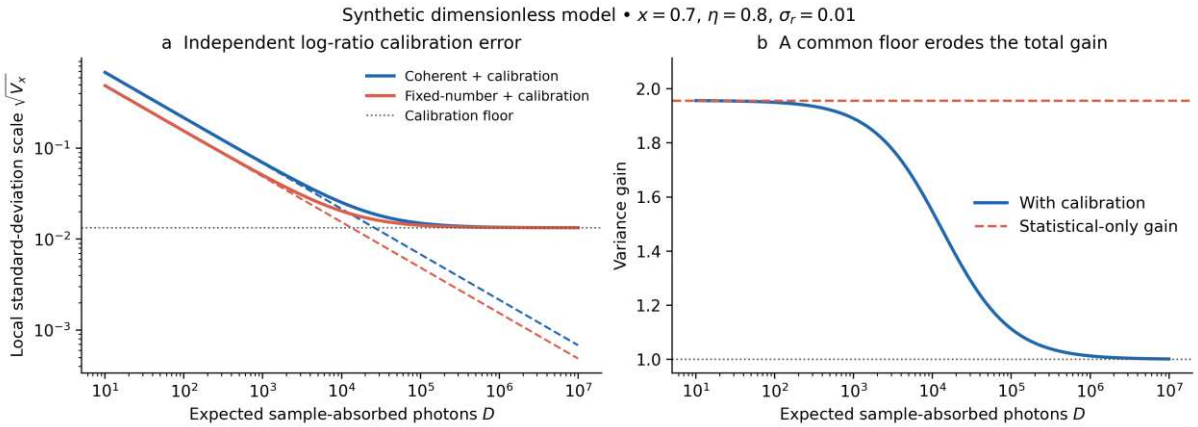


Figure 3. Spectral calibration limits the retained advantage. Synthetic example with $x = 0.7, \eta = 0.8$ and $\sigma_r = 0.01$. Solid curves include the auxiliary-calibration floor; dashed curves show statistical bounds alone. The right panel shows the fixed-dose variance advantage tending to unity. This does not imply that the fixed-target-precision exposure-saving ratio vanishes.

5 Discussion

5.1 What the analysis adds to established quantum sensing results

The Fock-state advantage in loss estimation and the use of a fixed specimen-photon resource are established results [4, 5, 16]. Quantum-enhanced concentration discrimination has also been demonstrated [17]. General nuisance-parameter theory explains why eliminating unknown parameters reduces useful information [18]. The present analysis does not rename any of these concepts as a new physical law. Its contribution is the explicit solution of a defined differential-concentration design problem: the throughput-adjusted bound, optimal absorbed-dose split, independent spectral-calibration floor, target-gain inequality and joint accounting-budget optimum are expressed in the same measurable parameters.

This distinction is important for comparison with nearby studies. Allen et al. optimize absorbance estimation through controllable interaction length [8]; here the path and wavelength pair are fixed while photon allocation and independent calibration resources are optimized. Goldberg and Heshami analyze dark counts in transmission estimation [11]; here the principal nuisance ambiguity

is between concentration and relative spectral throughput, with background treated as a separate extension. Woodworth et al. account for realistic quantum sources and transmission calibration [9, 10]; here an auxiliary calibration likelihood produces an explicit concentration-information floor and a retained-gain requirement. Ancilla-assisted strategies can change the available transmission information [19], but still require an identifiable connection between optical observables and the biochemical quantity.

The mathematical ingredients are standard, and combining them does not establish priority over every possible formulation in the literature. The resulting closed-form criteria provide a specific analytical contribution whose novelty should be judged against the stated problem, not against an exaggerated claim that quantum biosensing itself is new. No universal optimality over all quantum architectures is claimed.

5.2 Two different meanings of a useful advantage

A calibration floor erodes variance improvement at a fixed dose, but does not necessarily erase exposure savings at a fixed attainable precision. Equation (23) gives $D_{\mathrm{coh}}/D_{\mathrm{num}} = C/Q$ when both strategies share the same fixed calibration and the target lies above its floor. The denominator containing the calibration term cancels in this ratio. Near the floor both required doses become large, so the mathematical dose ratio alone does not guarantee practical usefulness.

This distinction prevents two opposite overinterpretations. It would be incorrect to announce that a photon-statistical advantage necessarily survives as a large total-precision improvement. It would also be incorrect to conclude that a calibration-limited apparatus can never save specimen exposure with quantum probes. Which advantage matters depends on whether an application fixes time, absorbed exposure, target uncertainty, total apparatus resources or an acceptable risk of sample alteration. Multiple passes and alternative optical geometries provide additional classical or quantum strategies that require their own sample-interaction accounting [20]. Our single-pass

coherent benchmark should not be called the best possible instrument under every resource definition.

5.3 Biomedical and biotechnological domain of applicability

The immediate application is a calibrated transmission assay for a single dominant absorbing species, or for a reaction whose differential absorption can be parameterized by one unknown concentration. Potential settings include purified biomolecular preparations, thin microfluidic channels and biochemical reaction aliquots. These are domains in which a known path length and a verified absorption spectrum may be obtainable. The equations provide a way to ask whether quantum-state preparation is justified after accounting for relative-response calibration, rather than selecting a quantum source solely because a sample is biologically important.

A real assay must supply experimentally justified k_i, true absorption fractions, background behavior and a stability model. The numerical coefficients in this work are deliberately not assigned to a particular analyte. Absorption by buffer or matrix can consume dose without supplying useful analyte information. Scattering and reflection remove photons from a collection channel without necessarily depositing their energy in the specimen; they cannot be inserted into $1 - t_i$ and automatically called absorbed dose. When absorption and detected transmission differ, the optimization remains applicable with separately determined positive d_i, but the simple identity $d_i = w_i(1 - t_i)$ must be replaced.

Intact tissue commonly requires multiple chromophores, heterogeneous paths and wavelength-dependent scattering. Those additional unknowns can make a two-channel model underdetermined. A quantum-enhanced detector does not increase the rank of an otherwise deficient spectral model. Similarly, unknown path length is confounded with concentration in Eq. (1) unless separately constrained. Additional wavelengths, time-resolved measurements or independent biochemical

information would be needed, with their photon costs included. Chemical processes that evolve during acquisition also need a time-dependent model [21].

5.4 Limitations and falsifiable extensions

The first limitation is source idealization. Perfect number statistics are assumed at the specimen. Heralding failures, unheralded exposure, multiphoton contamination and preparation loss can alter both information and dose. Experimental single-photon feed-forward work illustrates why these accounting details matter [22]. A credible extension would replace Eq. (4) with the measured incident photon-number distribution while retaining the same concentration, calibration and exposure definitions.

The second limitation is local design. The allocation depends on unknown parameters through p_i and d_i. A design can use a nominal operating point or a pilot estimate, but neither makes the parameter known. Robust or minimax designs over a concentration interval would be preferable when uncertainty in the operating point is large. They should be compared with the same robust coherent strategy, not with a deliberately misallocated reference.

Third, the Gaussian calibration likelihood assumes independence and a known information level. Common detector drift, correlations between sample and reference acquisition, or biased spectral interpolation can violate this assumption. A systematic error cannot be reduced merely by repeating a calibration without changing the source of the bias. Directly testing the stability of the log-response ratio is therefore a practical prerequisite for applying Eq. (22).

Fourth, the finite-background result is a first-order uncertainty-propagation approximation. Exact Fock-state inference in low-count or background-dominated regimes requires Eq. (28) or a more informative time-resolved likelihood. Detector dead time, afterpulsing and saturation are not included. Fifth, no patient safety threshold or therapeutic effect follows from an expected absorbed-photon count. Cell-damage measurements demonstrate the relevance of illumination wavelength,

intensity and mode, among other factors [23]. Biological validation would be needed before claiming improved viability or clinical benefit, although it is not required to establish the mathematical statements proved here.

A falsifiable theoretical extension is to choose a calibrated biomolecular spectrum, construct a fuller nuisance likelihood and test whether the retained-gain boundary in Eq. (22) remains conservative or fails under model mismatch. Failure would identify which physical assumption, rather than quantum mechanics itself, was responsible. Such an extension could use existing published spectral data with appropriate provenance before any new experimental apparatus is built.

6 Conclusions

For a two-wavelength linear absorption assay, quantum-enhanced concentration estimation requires both favorable photon statistics and an identifiable separation of concentration from instrumental spectral response. We derived the exact photon-counting Fisher bound with unknown common throughput, its optimal absorbed-dose allocation and the additive information penalty caused by finite independent relative-response calibration. These expressions yield a direct calibration requirement for retaining any specified variance advantage and a joint allocation rule for specimen and calibration resources.

The quantum-to-coherent variance gain can approach unity at high specimen dose when calibration information is fixed, while an exposure-saving ratio at a common attainable target precision can remain finite. This distinction is central to evaluating practical benefit. The numerical results are reproducible dimensionless illustrations of the theory, not biological measurements. The framework supports a specific decision: improve the quantum probe when photon statistics dominate, and improve spectral calibration when the biochemical inference is limited by its independent information floor.

Abbreviations

CRB, Cramér–Rao bound; QFI, quantum Fisher information; SI, International System of Units.

Declarations

Ethics approval and consent to participate

Not applicable. This theoretical study involves no human participants, animals, patient records or biological specimens.

Consent for publication

Not applicable. No identifiable personal data are included.

Availability of data and materials

All numerical results are generated from the equations and synthetic parameter choices reported in this article. The accompanying reproducibility package contains the complete Python script, numerical CSV files, figure files, software versions and numerical verification results. No external experimental dataset is used. No public repository deposit is claimed.

Funding

This research received no funding.

Competing interests

The authors declare that they have no competing interests.

Authors' contributions

Baldo Alberto Luigi Dalporto: Conceptualization, Formal analysis, Methodology, Visualization, Writing – original draft, Writing – review and editing, Project administration.

Sabine Mary: Visualization, Writing – review and editing.

Santiago Gallur: Supervision, Project administration, Writing – review and editing.

All authors approved the version prepared for submission and agree to be accountable for the work.

Author contact information

Corresponding author: Baldo Alberto Luigi Dalporto, baldo.dalporto@intec.edu.do

Use of generative artificial intelligence

OpenAI generative AI tools were used during preparation of the mathematical exposition, literature-search support, English-language editing, numerical code and figures. Responsibility for the submitted manuscript and approval of its final content remain with the named human authors. No experimental measurements were generated or represented as observed data.

References

1. M. A. Taylor, J. Janousek, V. Daria, J. Knittel, B. Hage, H.-A. Bachor, and W. P. Bowen. "Biological measurement beyond the quantum limit." Nature Photonics 7, 229–233 (2013). https://doi.org/10.1038/nphoton.2012.346

2. C. A. Casacio, L. S. Madsen, A. Terrasson, M. Waleed, K. Barnscheidt, B. Hage, M. A. Taylor, and W. P. Bowen. "Quantum-enhanced nonlinear microscopy." Nature 594, 201–206 (2021). https://doi.org/10.1038/s41586-021-03528-w

3. A. Monras and M. G. A. Paris. "Optimal Quantum Estimation of Loss in Bosonic Channels." Physical Review Letters 98, 160401 (2007). https://doi.org/10.1103/PhysRevLett.98.160401

4. G. Adesso, F. Dell'Anno, S. De Siena, F. Illuminati, and L. A. M. Souza. "Optimal estimation of losses at the ultimate quantum limit with non-Gaussian states." Physical Review A 79, 040305(R) (2009). https://doi.org/10.1103/PhysRevA.79.040305

5. P.-A. Moreau, J. Sabines-Chesterking, R. Whittaker, S. K. Joshi, P. M. Birchall, A. McMillan, J. G. Rarity, and J. C. F. Matthews. "Demonstrating an absolute quantum advantage in direct absorption measurement." Scientific Reports 7, 6256 (2017). https://doi.org/10.1038/s41598-017-06545-w

6. E. Losero, I. Ruo-Berchera, A. Meda, A. Avella, and M. Genovese. “Unbiased estimation of an optical loss at the ultimate quantum limit with twin-beams.” Scientific Reports 8, 7431 (2018). https://doi.org/10.1038/s41598-018-25501-w

7. R. Whittaker, C. Erven, A. Neville, M. Berry, J. L. O’Brien, H. Cable, and J. C. F. Matthews. “Absorption spectroscopy at the ultimate quantum limit from single-photon states.” New Journal of Physics 19, 023013 (2017). https://doi.org/10.1088/1367-2630/aa5512

8. Allen EJ, Sabines-Chesterking J, McMillan AR, Joshi SK, Turner PS, Matthews JCF. Approaching the quantum limit of precision in absorbance estimation using classical resources. Physical Review Research. 2020;2:033243. https://doi.org/10.1103/PhysRevResearch.2.033243

9. Woodworth TS, Chan KWC, Hermann-Avigliano C, Marino AM. Transmission estimation at the Cramér-Rao bound for squeezed states of light in the presence of loss and imperfect detection. Physical Review A. 2020;102:052603. https://doi.org/10.1103/PhysRevA.102.052603

10. T. S. Woodworth, C. Hermann-Avigliano, K. W. C. Chan, and A. M. Marino. “Transmission estimation at the quantum Cramér-Rao bound with macroscopic quantum light.” EPJ Quantum Technology 9, 38 (2022). https://doi.org/10.1140/epjqt/s40507-022-00154-x

11. A. Z. Goldberg and K. Heshami. “Optimal transmission estimation with dark counts.” Measurement Science and Technology 34, 045701 (2023). https://doi.org/10.1088/1361-6501/acaf12

12. Zhang Z, Zhang X, Liu J, Dong H. Quantum-Enhanced Weak Absorption Estimation with Correlated Photons. Physical Review Letters. 2025;134:133604. https://doi.org/10.1103/PhysRevLett.134.133604

13. Minati G, Urbani E, Spagnolo N, Cimini V, Sciarrino F. Multiparameter quantum-enhanced adaptive metrology with squeezed light. Nature Communications. 2026;17:6418. https://doi.org/10.1038/s41467-026-73069-1

14. P. P. Laissue, R. A. Alghamdi, P. Tomancak, E. G. Reynaud, and H. Shroff. "Assessing phototoxicity in live fluorescence imaging." Nature Methods 14, 657–661 (2017). https://doi.org/10.1038/nmeth.4344

15. S. L. Braunstein and C. M. Caves. "Statistical distance and the geometry of quantum states." Physical Review Letters 72, 3439–3443 (1994). https://doi.org/10.1103/PhysRevLett.72.3439

16. R. Nair. "Quantum-Limited Loss Sensing: Multiparameter Estimation and Bures Distance between Loss Channels." Physical Review Letters 121, 230801 (2018). https://doi.org/10.1103/PhysRevLett.121.230801

17. K. Matsuzaki and T. Tahara. "Superresolution concentration measurement realized by sub-shot-noise absorption spectroscopy." Nature Communications 13, 953 (2022). https://doi.org/10.1038/s41467-022-28617-w

18. J. Suzuki. "Nuisance parameter problem in quantum estimation theory: tradeoff relation and qubit examples." Journal of Physics A: Mathematical and Theoretical 53, 264001 (2020). https://doi.org/10.1088/1751-8121/ab8672

19. J. Wang, R. L. de Matos Filho, G. S. Agarwal, and L. Davidovich. “Quantum advantage of time-reversed ancilla-based metrology of absorption parameters.” Physical Review Research 6, 013034 (2024). https://doi.org/10.1103/PhysRevResearch.6.013034

20. T. Juffmann, B. B. Klopfer, T. L. I. Frankort, P. Haslinger, and M. A. Kasevich. “Multi-pass microscopy.” Nature Communications 7, 12858 (2016). https://doi.org/10.1038/ncomms12858

21. V. Cimini, I. Gianani, L. Ruggiero, T. Gasperi, M. Sbroscia, E. Roccia, D. Tofani, F. Bruni, M. A. Ricci, and M. Barbieri. “Quantum sensing for dynamical tracking of chemical processes.” Physical Review A 99, 053817 (2019). https://doi.org/10.1103/PhysRevA.99.053817

22. J. Sabines-Chesterking, R. Whittaker, S. K. Joshi, P. M. Birchall, P. A. Moreau, A. McMillan, H. V. Cable, J. L. O’Brien, J. G. Rarity, and J. C. F. Matthews. “Sub-Shot-Noise Transmission Measurement Enabled by Active Feed-Forward of Heralded Single Photons.” Physical Review Applied 8, 014016 (2017). https://doi.org/10.1103/PhysRevApplied.8.014016

23. S. Wäldchen, J. Lehmann, T. Klein, S. van de Linde, and M. Sauer. “Light-induced cell damage in live-cell super-resolution microscopy.” Scientific Reports 5, 15348 (2015). https://doi.org/10.1038/srep15348